Preprint Title	Radular tooth coating in members of Dendronotidae and Flabellinidae (Nudibranchia, Gastropoda, Mollusca)
Authors	Wencke Krings, Stanislav N. Gorb, Charlotte Neumann and Heike Wägele
Publication Date	23 Apr. 2024
Article Type	Full Research Paper
Supporting Information File 1	Supplementary Material.pdf; 1.3 MB
ORCID® iDs	Wencke Krings - https://orcid.org/0000-0003-2158-9806; Stanislav N. Gorb - https://orcid.org/0000-0001-9712-7953; Heike Wägele - https://orcid.org/0000-0001-6899-0336

Radular tooth coating in members of Dendronotidae and Flabellinidae (Nudibranchia, Gastropoda, Mollusca)

Wencke Krings[1,2,3,4*], Stanislav N. Gorb[4], Charlotte Neumann[1,2,3], Heike Wägele[5]
[1] Department of Cariology, Endodontology and Periodontology, Universität Leipzig, Liebigstraße 12, 04103 Leipzig, Germany
[2] Department of Electron Microscopy, Institute of Cell and Systems Biology of Animals, Universität Hamburg, Martin-Luther-King-Platz 3, 20146 Hamburg, Germany
[3] Department of Mammalogy and Palaeoanthropology, Leibniz Institute for the Analysis of Biodiversity Change, Martin-Luther-King-Platz 3, 20146 Hamburg, Germany
[4] Department of Functional Morphology and Biomechanics, Zoological Institute, Christian-Albrechts-Universität zu Kiel, Am Botanischen Garten 1-9, 24118 Kiel, Germany
[5] Department of Phylogenetics and Evolutionary Biology, Leibniz Institute for the Analysis of Biodiversity Change, Adenauerallee 160, 53113 Bonn, Germany

*corresponding author: wencke.krings@uni-hamburg.de

Abstract
Nudibranchs, with their mesmerizing diversity and ecological significance, play crucial roles in marine ecosystems. Central to their feeding prowess is the radula, a chitinous structure with diverse morphologies adapted to prey preferences and feeding strategies. This study focuses on elucidating wear coping mechanisms in radular teeth of carnivorous molluscs, employing *Dendronotus lacteus* (Dendronotidae) and *Flabellina affinis* (Flabellinidae) as model species. Both species forage on hydrozoans. Through scanning electron microscopy, confocal laser scanning microscopy, nanoindentation, and energy-dispersive X-ray spectroscopy, the biomechanical and compositional properties of their teeth were analysed. Results revealed distinct autofluorescence patterns and elemental compositions correlating with mechanical properties. Notably, tooth coatings, composed of calcium and silicon and high hardness and stiffness compared to the inner tooth structure, with varying mineral contents across tooth regions and ontogenetic zones, were found. The findings suggest that tooth mechanical properties are intricately linked to species ecology and function, with teeth adapted to prey type and feeding behaviors. Moreover, the presence of Ca and Si in the tooth coating highlight their role in enhancing wear resistance. Overall, this study provides valuable insights into the biomechanical adaptations of nudibranch radular teeth, shedding light on the intricate interplay between tooth structure, elemental composition, and ecological function in marine molluscs.

Keywords
Molluscs, elemental composition, biomineralization, feeding, mechanical properties

Introduction

Nudibranchs, a captivating group of marine gastropod mollusks, have long time fascinated scientists and enthusiasts alike due to their striking diversity in morphology, behavior, and ecological roles. With over 3,000 described species, nudibranchs exhibit an astonishing array of colours, shapes, and patterns, making them iconic inhabitants of marine ecosystems worldwide. Beyond their aesthetic appeal, nudibranchs play vital roles in marine food webs and ecosystem dynamics, largely driven by their diverse feeding ecology [e.g., 1].

Their feeding habits encompass a broad spectrum, including herbivory, carnivory, scavenging, and symbiosis with photosynthetic organisms [e.g., 2–12]. By targeting various prey items, such as sponges, bryozoans, tunicates, cnidarians, nudibranchs occupy diverse ecological niches and play crucial roles in controlling prey populations and shaping benthic communities. Furthermore, nudibranchs have evolved fascinating mechanisms for obtaining and processing food, ranging from specialized radular structures to chemical defenses derived from ingested prey. Understanding nudibranch diversity and feeding ecology not only sheds light on the intricacies of marine ecosystems, but also underscores the importance of conserving these fascinating creatures and their habitats.

Food gathering is mainly performed by the radula, a characteristic feature of molluscs, consisting of a chitinous membrane, in which rows of teeth are embedded. These teeth display adaptations in morphology and arrangement based on the preferred ingesta (i.e., food, prey items, particles on the food, substrate to which the food is attached, etc.), as evidenced in various studies [13–24]. The radula is comprised of tightly packed chitin fibres and associated proteins, which extend from the membrane to the tooth base, stylus, and ultimately to the cusps [25, 26]. Across different molluscan species, the membrane and teeth may be accompanied by odontophoral cartilages on either side, facilitating the bending of the radula, which leads to a certain 3-dimensional tooth arrangement. In addition, the radula is supported by cartilages of different sizes and shapes depending on the species. Muscles associated with feeding movements control the radula, allowing for precise and coordinated feeding actions. Food particles are then retained by adhesive forces of the saliva [27]. In some taxa, the radula co-operates with chitinous plates, the jaws, which reinforce the foregut and act as a counterpart to the radula to cut and hold the ingesta.

During feeding activities, like piercing or scratching, radular teeth must transfer high forces onto hard target surfaces, leading to strong stress concentrations, without experiencing significant structural failure. This is facilitated by tooth morphology, such as providing broad and thick cusps during scratching actions, or by mechanical property gradients along the tooth structure, typically with the cusp or tip being the stiffest region and the embedment in the membrane being the most flexible region [e.g., 17,28–44]. This arrangement increases strain at the base, reducing stress values at the tooth tip, when interacting with food, while simultaneously allowing for bending or swerving, when stress becomes too high. Furthermore, in certain taxa, this bending enables teeth from adjacent rows to interlock [17,45,46], distributing stress across multiple teeth, a phenomenon recently studied experimentally and termed the "collective effect" [20,37,47]. Mechanical property gradients, facilitating this biomechanical behavior, can stem from various factors, including tooth morphology (e.g., ratio of its width to its height), distribution of inorganic compounds (more minerals at the cusp) [e.g., 30–32,37,48–55], distribution of proteins, degree of tanning and cross-linking of chitin [34,37–40,56–58], chitin fiber density [26], and water content of teeth and radular membrane [20,37,47]. Finally, radular supporting structures like odontophoral cartilages and radular bolsters [e.g., 59–61] appear to support the radular membrane and reduce stress concentration by acting as a cushion or muscular hydrostat [22,62–66].

Teeth and membrane are continuously produced in the building zone or the radular sac, undergoing maturation during their course towards the radular working zone [see e.g., 12,67–69], where they directly act onto the ingesta. Over time, the utilized teeth are shed in the degenerative zone. Despite the constant renewal of the radula, certain wear coping mechanisms aim at reducing wear and structural failure. In members of Polyplacophora [30,37,49–51,53–55], Cephalopoda [44], and members of the gastropod groups Patellogastropoda [e.g. 31,32,48,52], Paludomidae [26,70], Cephalaspidea [39], and some Nudibranchia [40], this involves the incorporation of elevated levels of iron (Fe), calcium (Ca), or silicon (Si) into the superficial regions of teeth that interact with ingesta. This results in harder tooth cusps capable of withstanding hard and abrasive ingesta, like Porifera spiculae, crustacean carapaces, Foraminifera, or algae attached to stone surfaces. In Polyplacophora and Patellogastropoda, the tooth cusps of the dominant teeth are filled with such incorporations, whereas in the examined cephalopod, paludomid, heterobranch and nudibranch taxa, only a thin outer layer with high concentrations of Ca or Si is present on the tooth cusps, which seems to reduce abrasion. Despite of these studies, wear coping mechanisms are, however, understudied.

In this study, we elucidate wear coping mechanisms in radular teeth of two members of the Nudibranchia. As model species, we used *Dendronotus lacteus* (Thompson, 1840) (Dendronotidae), and *Flabellina affinis* (Gmelin, 1791) (Flabellinidae), both primarily feeding on hydrozoans [71,72]. With regards to radular teeth, taxa from these genera were previously investigated in the context of radular formation [67,69], the fine morphology of the radular apparatus [73], and trophic specialisation [74]. Biomechanical and compositional properties of the teeth of both species are here assessed using a variety of methodological approaches, including scanning electron microscopy (SEM), confocal laser scanning microscopy (CLSM), nanoindentation, and energy-dispersive X-ray spectroscopy (EDX, EDS). To determine, how well the coating is bound in the chitin-protein composite material of teeth and how the reduction in Ca and Si content might affect the material properties of the coating, some *D. lacteus* radulae were treated with acid and then tested. Based on the findings, a hypothesis about the interaction between ingesta and radular teeth was formulated.

Results

Morphology and wear of teeth nanostructure

By SEM examination, we observed that the *Dendronotus lacteus* specimen typically possess approximately 6–8 lateral teeth per row on each side of the prominent central tooth. Lateral teeth are very often smooth. The central rhachidian tooth shows small denticles (Figure 3). *Flabellina affinis* possess one prominent central tooth, flanked to each side by one large lateral tooth (Figure 4). The central teeth bear strong denticles and the lateral ones pointy ones. In both species, the inner tooth structure was fibrous (Figure 3H). The tooth surface towards the membrane was covered by an extremely thin smooth outer layer, measuring no more than 100 to 200 nm in thickness, and devoid of fibres (Figure 3G, only *D. lacteus* depicted). Conversely, the tooth surface towards the membrane was rather smooth and fibrous (Figure 3E).

Autofluorescence signals

In both species, mature teeth displayed a consistent autofluorescence pattern. In the natural radulae from *D. lacteus*, teeth predominantly emitted a vibrant green signal (Figure 5A). At the tips of the central teeth and the central sides of the lateral teeth, the areas emitted blue autofluorescence. In the demineralized radulae of *D. lacteus*, which were documented with the same settings as the natural radulae, the central tooth tips emitted fewer blue autofluorescence (Figure 5B). In the central teeth of *F. affinis*, the tips and the cusps to the oral cavity emitted a blue signal, while the tips and the cusps to the membrane displayed a prominent green fluorescence (Figure 5C). In the lateral teeth, the blue and green signals are rather mixed.

Mechanical properties

The Young's modulus (E) delineates the stiffness of a solid material and signifies the relationship between tensile stress and axial strain. This mechanical parameter reflects the material's capacity to transmit force and withstand failure. The hardness (H) is the measure of the resistance to local plastic deformation induced by indentation or abrasion.

In the case of *D. lacteus* and *F. affinis*, all radulae displayed a notably strong positive correlation between E and H ($r = 0.94–1.00$, $p<0.0001$*; see Supplementary Tables 1–10). *D. lacteus* and *F. affinis* possessed teeth with similar E and H values (see Figure 6 and Supplementary Tables 11–12 for means and standard deviations). In both species, E and H values increased during ontogeny from the building zone to the maturation zone (Figure 6; Supplementary Tables 11–12). From the maturation zone to the working zone, however, mean values decreased.
In each species, the central teeth were harder and stiffer than the lateral ones. Upon comparing the inner structures of the central and lateral teeth, similar H and E values were observed for both species (Figure 6; Supplementary Tables 11–12). The coating of the teeth was always highly significantly harder and stiffer than the inner tooth material with regard to both parameters in all ontogenetic zones

(Figure 6). With regard to the tooth coating of the central teeth in *D. lacteus*, the tip was highly significantly harder and stiffer than the cusp in both the building and working zone. In the maturation zone of this species, tip and cusp were not different. In *F. affinis*, the coating of the tip and the cusp of the central tooth were not different in the maturation and working zone, but were highly significantly softer and more flexible in the building zone (Figure 6). With regard to the coatings of the lateral teeth, the central sides in the working zones were always significantly harder and stiffer than their lateral sides. In the maturation zone, most central sides were significantly harder and stiffer than the lateral ones. In the building zone, the mechanical properties of the sides were rather similar and did not show many differences. The coatings of the tips were, in the mature teeth, harder and stiffer, followed by the coatings of the styli and the bases (Figure 6).
The teeth in partially demineralized radulae were softer and more flexible than those of the natural radulae (see Figure 7 and Supplementary Table 11 for means and standard deviations).

Elemental composition
The elemental compositions of the inner tooth structure and the tooth coatings were assessed using EDX, which is, however, not capable to determine the bounding conditions of the elements. We found for both species, that most elements (Cl, Cu, Fe, K, Mg, P+Pt, S, and Zn) were present in small proportions (<1 atomic %) (see Figure 8 and Supplementary Tables 13–16 for means and standard deviations). With regard to Ca and Si, their contents in the inner tooth structure were also <1 atomic %. However, they were significantly higher in the coating (up to 12 atomic %, depending on the region) (Figure 8; Supplementary Tables 13–16). This was observed in both species.
The Ca content of the central teeth was highest in the tooth tip coating, whereas the Si content was highest in the cusp coating (Figure 9; Supplementary Tables 13–16). In the lateral teeth, the coatings of the central sides contained more Ca, whereas the coatings of the lateral sides contained significantly more Si.
When Ca and Si were sorted to orientation of the teeth, the tooth coatings towards the membrane always contained significantly less Si and Ca than the tooth coatings towards the oral cavity (Figure 10; Supplementary Tables 13–16).
Content of the elements increased from the building zone to the maturation zone, but from the maturation to the working zone most mean values decreased (Figures 8–10).
Demineralization of the radulae resulted in lesser amounts of the discussed elements (see Figure 11 and Supplementary Tables 13–14 for means and standard deviations).

Relationship between autofluorescence, elemental composition and mechanical properties
Our analysis revealed strong to very strong positive correlations between the values of the Young's modulus E and the hardness H with the content of calcium (Ca), silicon (Si), and the sum of Ca and Si (see Figure 12 for relationship and Supplementary Tables 1–10 for correlation coefficients). This relationship was also detectable in the partially demineralized radulae.

Discussion
This is the first time that two individuals of the nudibranch taxon Cladobranchia are investigated. *Dendronotus lacteus* (Dendronotidae) is a member of the Dendronotida, a group known to mainly feed on hydrozoan species, especially members of the Thecata. *Flabellina affinis* (Flabellinidae) belongs to the Aeolidida, where most members are feeding on athecate members of the Hydrozoa.

Properties of the tooth material
The mechanical characteristics of materials play a pivotal role in shaping the mechanical behavior of biological structures. Young's modulus (E) is a measure of tensile or compressive stiffness, representing a material's capacity to transfer force and the resistance to fail during e.g. puncturing [75–79; for review on puncture mechanics see 80]. The hardness (H) on the other hand, quantifies the resistance to local plastic deformation induced by indentation or abrasion. Given the diverse forces and types of

ingesta encountered during foraging [47,65,66,81–83], molluscan teeth exhibit different mechanical properties that reflect their specific functions and ecological niches.

Functional gradients and variations in biological materials can arise from various factors such as the structure's architecture, degree of tanning, and inorganic content [for review, see 84]. In chiton and limpet radular teeth, these gradients are mostly influenced by the high mineral content [for reviews, see 85–87], while in partially demineralized radular teeth, mechanical properties seem to be influenced by chitin fiber architecture, the distribution of proteins and degree of tanning [26,38].

While our understanding of the mechanical properties of molluscan radular teeth still remains incomplete, existing data suggest that E and H values, along with the presence or absence of gradients within each tooth, are intricately linked to species ecology. Species feeding on soft ingesta (i.e., algae grazed from soft substrates like sand or mud) typically possess softer and more flexible teeth (values of the inner tooth structure: $E \leq 8$ GPa and $H \leq 1$ GPa) [43], capable of deforming to reduce the risk of structural failure and facilitate particle gathering. Animals specialised on solid ingesta, as members of the Polyplacophora, Fissurellidae, Patellogastropoda, and paludomid gastropods, foraging on algal films covering rocks, or have some interactions with hard ingesta, as the nudibranch gastropods *Felimare picta* and *Doris pseudoargus* feeding on Porifera with hard spiculae, the cephalaspidean gastropod *Gastropteron rubrum* feeding on Foraminifera, or the cephalopod *Loligo vulgaris* piercing crustacean carapaces have harder and stiffer teeth, better equipped to withstand higher forces without failure.
The lateral teeth of the polyplacophoran *Cryptochiton stelleri* and *Lepidochitona cinerea* are nearly the stiffest and hardest teeth described, with E values ranging from 30 to 130 GPa and H from 4 to 12 GPa. High contents of inorganic components between the chitin fibres are responsible for the elevated values [30,37,88]. Due to the abundant incorporation of silica, the dominant teeth of *Patella vulgata* (Patellogastropoda) can even exceed these values (E: 52–150 GPa; H: 3–7 GPa) [31,32]. Partially demineralized teeth, such as those found in the vetigastropod *Megathura crenulata* with a broad food spectrum, exhibit greater flexibility. Here, the chitin fibres are cross-linked by Ca- and Mg-ions and lack substantial mineral content (E of the inner tooth structure: 16 GPa) [34]. The teeth of Porifera-consuming Nudibranchia and of the cephalopod *L. vulgaris*, which also have low inorganic content, display similar E and H values (values of the inner tooth structure: nudibranchs *F. picta* and *D. pseudoargus*: E = ~5–15 GPa, H = ~0.1–0.9 GPa [40]; of *L. vulgaris*: E = 2–9 GPa, H = 0.07–0.38 [44]). Teeth of the cephalaspid *G. rubrum* and some paludomid gastropods foraging on solid ingesta are also softer and more flexible compared to members of the Polyplacophora and Patellogastropoda (values of the inner tooth structure: *G. rubrum*: H = ~0.1–1.0 GPa and E = ~1–17 GPa [39]; paludomids: H = ~0.4 GPa and E = ~8 GPa [35,36,38,43]). Despite their softer nature, however, these teeth can distribute stress between rows, allowing them to withstand forces similar to highly mineralized teeth of Polyplacophora ("collective effect" [20,22,37,47]).
The teeth of the here studied nudibranch species *Dendronotus lacteus* and *Flabellina affinis* contain comparably low contents of Ca, Si, Zn, Cu, etc. in their inner structure. The values for E and H are comparable to the values of the teeth of paludomids that feed on soft substrates. This can be explained by the nature of the diet of the species studied here, which consists of relatively soft and flexible food components. They feed mainly on hydrozoans, whose tissues show no calcification or further mineralisation.

The mechanical properties are also related to the function of the radular teeth. Tooth morphologies and mechanical properties may be similar or may vary within one row, which indicates that the teeth on the radular membrane either have a similar function ("monofunctional" radula) or distinct functions ("multifunctional" radula [40,43]). In certain molluscs, like Polyplacophora and limpets, the lateral teeth (dominant teeth) differ significantly from the central and marginal ones [37]. These dominant teeth irrespective of their position in the radular rows exhibit exceptional hardness and stiffness values allowing them to reduce wear during interaction with rocks. The other teeth likely play a role in gathering loosened food particles and transporting them into the mouth cavity. A similar pattern was determined in paludomid gastropods foraging on solid ingesta, where the central teeth are the stiffest and hardest elements, followed by the lateral, and finally the marginal teeth [35,36,38,43]. Their central and lateral teeth probably loosen the algae from rocks, whereas the marginal teeth collect the particles. In *G. rubrum*, the teeth also have different functions, with some teeth being primarily responsible for grasping and holding the ingesta, while others have a supporting function as bolsters [39]. In *Dendronotus lacteus* and *Flabellina affinis*, the mechanical properties of the central and lateral teeth are similar, which indicates that the tooth materials have to withstand similar stresses. As the central teeth are broader and have a larger attachment area with the membrane, these teeth are probably capable of transferring higher forces onto the ingesta surface than the laterals. The prey item is probably first grasped (and perhaps even cut) by the elongated free edges of the large jaws. Then, the tips of the central teeth from the active radular region pierce and tear the prey, so that larger pieces can be transported into the oral cavity during radular retraction. The lateral teeth, which are longer and thinner, probably support this process by piercing or stabilizing the prey parts from the sides.

Coating

Wear prevention has been extensively documented for Polyplacophora and Patellogastropoda teeth, where high proportions of Fe and Si are incorporated into the thick interacting edges of the dominant teeth (i.e. leading edges [see e.g., 30–32,48–55,89]). In almost unmineralized teeth of the nudibranch gastropods *D. pseudoargus* and *F. picta*, some paludomids, the heterobranch gastropod *G. rubrum*, and the cephalopod *L. vulgaris*, a similar wear-coping mechanism involving high proportions of Ca or Si on the interacting surfaces has been observed [37,39,40,70]. In comparison to polyplacophoran and patellogastropod teeth, which are fully packed with iron oxides or silica, these teeth possess, however, only a thin superficial layer. This layer is significantly harder and stiffer than the inner tooth structure (documented for *D. pseudoargus* and *F. picta*: $E_{max.}$ = 45 GPa and $H_{max.}$ = 2.3 GPa [40]), potentially reducing abrasion during interactions with substrates. For *D. lacteus* and *F. affinis,* we documented a thin superficial layer with high content of Ca and Si as well, which was also observed at fractures in SEM images. This coating was especially prominent on the tooth surfaces, which were oriented towards the oral cavity and thus have an intimate interaction with the ingesta. Interestingly, we detected that Ca and Si were not evenly distributed across the tooth surface, but was distributed in a clear pattern. It is possible that the cells that secrete the central side of the lateral tooth covering and the central tooth tip surfaces provide more Ca, while the cells that secrete the lateral side of the lateral tooth covering and the central tooth cusps tend to provide more Si. This, however, needs further investigations. By nanoindentation we were able to determine the *E* and *H* values of the coating towards the oral cavity, which were significantly higher than the values of the inner tooth structure. The *E* and *H* values of the coating were, however, noticeably lower than the coating of the Porifera-consuming nudibranchs *D. pseudoargus* and *F. picta*. These differences can be explained by the different ingesta of the latter species. Teeth of *D. pseudoargus* and *F. picta* are more prone to wear, as they can interact with the hard silicate spiculae of the sponges, whereas the cuticular parts of the prey of *D. lacteus* and *F. affinis* are less abrasive. We determined that the central coating of the lateral teeth is harder and stiffer than their lateral coating. During piercing, the central sides of the teeth potentially have more frequent and more intimate interactions with the ingesta, which require a higher degree of abrasion resistance.

To document the degree of tanning and the distribution of proteins, a method using laser excitation by CLSM was previously established on arthropods [90], which revealed autofluorescence signals relating to material composition [see e.g., 91]. In arthropods, the emitted autofluorescence signal relates to the following composition: blue signals are related to high proportions of resilin or other matrix proteins. Red signals are related to sclerotized cuticle and green signals to weakly-sclerotized chitin. When, however, higher mineral content is present, the CLSM signal can be corrupted: blue signals then can be related to high Ca content, as was shown for crustaceans [92–94] and the Porifera-consuming nudibranch *D. pseudoargus* [40]. Green can indicate a high content of Si, as documented in Porifera-consuming nudibranch *F. picta* [40], the heterobranch *G. rubrum* [39], and the cephalopod *L. vulgaris* [44]. In the here studied species, we found, that the regions of the teeth emitting a strong blue autofluorescence contain higher proportions of Ca in their coatings. The regions with high Si-content in the tooth coating related to a strong green signal, which highlight the importance of implementing elemental analyses in addition to CLSM imaging in the case of mineralised or metal ions bearing tissues.

Our analysis revealed positive correlations between the mechanical properties (Young's modulus and hardness) and the content of Ca and Si in the radular tooth coating, despite the smaller proportions of elements, when compared to other molluscs. The presence of certain elements, like Ca, P, Cl, and F, suggests the presence of apatite, a mineral found in various molluscan radular teeth [e.g., 51,53,95–100]. Other elements, like Mg, K, S [e.g., 57,101,102] or Cu, Fe, and Zn, may also contribute to stiffness and hardness, even though the contents of the here studied species are rather small in comparison to the previously examined chiton and limpet taxa [e.g., 37,54,89,99,100,103–108]. Si, probably in the form of silica [e.g., 86,96,97,100,104,109,110], appears to enhance the mechanical properties of the tooth coating of the here studied two Nudibranchia species. This assumption is supported by the observation that the mechanical properties values still correlate with the elemental content, when the teeth are partially demineralized.

In our study, we found out that in the working zone, elemental content together with E and H values decreased, compared to the maturation zone. A reduction in biomineral content indicates chemical wear, which contributes to decay and potential loss of functionality. This decline may be attributed to the leaching of elements by surrounding water or saliva. Saliva, known to be slightly or highly acidic in gastropods, especially in carnivorous ones, aids in extra intestinal digestion [e.g., 111–115]. This acidity could explain the decrease observed in the working zone of the radula in the two species studied. This pattern during ontogeny was previously also reported for the carnivorous gastropod *Anentome helena* [116]. Saliva also contains enzymes, such as aminopeptidase [115], which additionally could damage tooth material and enhance element leaching. However, the pH values and composition of saliva remain unknown across species. Further investigation is needed to understand the impact of saliva on the elemental composition of radular teeth during their formation.

In the present study, we found out, that despite differences in the morphology of the radulae, the mechanical properties and the tooth compositions are similar in both species. Further studies are needed to investigate, whether these similarities are related to phylogeny and are ancestral in Cladobranchia or rather to the feeding ecology, which might have triggered convergent evolution of tooth structures. Increasing the number of cladobranch species could provide stronger insights into this scientific problem.

Material & Methods

Specimens and preparation

Individuals of *Dendronotus lacteus* were collected between 1964 and 1966 by Annetrudi Kress in Plymouth, England and fixed in 80% EtOH. *Flabellina affinis* was collected by Heike Wägele at Mataró, Spain on 05/23/2006 and fixed in formaldehyde and later transferred to 80% EtOH. 17 adult specimens of *D. lacteus* and 10 of *F. affinis* were dissected. Radulae were carefully extracted and cleaned with a brief ultrasonic bath in 80% ethanol. These were first analysed to confirm the identification based on external characteristics. To receive partially demineralized radulae, six radulae of *D. lacteus* were placed in acetic acid (100%, Carl Roth GmbH & Co. KG, Karlsruhe, Germany) for two days.

For the central (rhachidian) teeth, we differentiated between the tips and the cusps, and for the lateral teeth, between the bases, styli, and the tips (see Figure 1 for regions). The lateral teeth consist of a central/medial side, i.e. facing the central (rhachidian) tooth, and a lateral side, which faces outwards. CLSM and SEM documentation was performed with the intact and whole radula. EDX analyses of the inner tooth structure were performed with embedded radulae (see below) and of the tooth surface (coating) with whole teeth. The latter analysis was conducted at the tooth coating towards the membrane and the coating towards the oral cavity (Figure 1). Nanoindentation was performed on the inner tooth structure of embedded radulae (see below) and of the tooth coating with whole teeth. The latter analysis was only performed with the coatings facing towards the oral cavity. A summary of the workflows is depicted in Figure 2.

Confocal laser scanning microscopy

To capture the natural fluorescence of the tooth material by confocal laser scanning microscopy (CLSM), we prepared two cleaned radulae per group (*D. lacteus*, *F. affinis*, demineralized *D. lacteus*) on glass slides following the method outlined by [90]. Each radula was enclosed by multiple reinforcement rings filled with glycerine (99.5% or higher purity, water-free, Carl Roth GmbH & Co. KG, Karlsruhe, Germany) and covered with a glass slip. Following the procedure described by [38,100], we documented the samples using a Zeiss LSM 700 confocal laser scanning microscope (Carl Zeiss Microscopy GmbH, Jena, Germany). Four stable solid-state lasers emitting at 405 nm, 488 nm, 555 nm, and 639 nm wavelengths were utilized. Specific bandpass or longpass emission filters (ranging from 420–480 nm, 490 nm or higher, 560 nm or higher, and 640 nm or higher) were employed accordingly. The four *D. lacteus* radulae were scanned with the same settings to enable comparison between the natural and demineralized radulae. Post-scanning, the autofluorescence images were combined (using maximum intensity projection) with Zeiss Efficient Navigation (Zen) software (Carl Zeiss MicroImaging GmbH). Finally, we assigned blue color to the autofluorescence signal from the 405 nm laser, green to 488 nm, and red (50% saturation) to both 555 nm and 639 nm. Afterwards, the radulae were cleaned in 70% EtOH in an ultrasonic bath to remove the glycerine and used for SEM (Figure 2).

Scanning electron microscopy and 3D visualization

To document the morphology of the radulae using scanning electron microscopy (SEM), the radulae from CLSM and, additionally, four radulae of each species and two demineralized radulae (Figure 2) were attached onto SEM specimen holders using double-sided adhesive carbon tape, air-dried and coated with a 5 nm layer of platinum. We utilized a SEM Zeiss LEO 1525 (One Zeiss Drive, Thornwood, NY, USA) for visualization. To document the orientation of the teeth in a more natural environment, we critically point-dried two radulae of *D. lacteus* and one of *F. affinis* that were still embedded in the odontophoral cartilage. These radulae were treated with a series of increasing alcohol concentrations (80%, 90%, 100%, 100% EtOH, for 1 h each) and then placed in a 1:1 solution of 100% EtOH and 100 % acetone, followed by 100 % acetone (for 1 h each). Critical point drying with carbon dioxide was performed with the Leica EM CPD300 (Leica Camera AG, Wetzlar, Germany) at 20 cycles. Afterwards, samples were attached to SEM sample holders, sputter-coated and visualized with the SEM Zeiss LEO. For three-dimensional (3D) visualization of *D. lacteus* radula (Figure 1), the SEM images were used. With Blender v2.83 software (Blender Foundation, Amsterdam, Netherlands), the teeth were manually modelled while constantly comparing the 3D visualization with SEM images captured from the various perspectives. This process was conducted in a manner consistent with the protocol previously outlined in [19,66].

Energy dispersive X-ray spectroscopy

To analyse the elemental composition of the inner tooth structure (inside) by energy dispersive X-ray spectroscopy (EDX, EDS), we used three radulae of *D. lacteus*, three of *F. affinis*, and two demineralized ones, which were all previously documented by SEM. Overall, we tested 1721 small areas by EDX (see below).

Following our established procedure [100,116,117], we attached these radulae to glass slides using double-sided adhesive tape. Each radula was encircled by a small metallic ring, which was then filled with epoxy resin (Reckli Epoxy WST, RECKLI GmbH, Herne, Germany) to completely cover the radula. After allowing the resin to polymerize for three days at room temperature, we removed the glass slides and adhesive tape. The samples were then polished using sandpapers of varying roughness until the cross-sections of the teeth were visible, and further smoothed with a suspension of aluminium oxide polishing powder with a grain size of 0.3 µm on a polishing machine (Minitech 233/333, PRESI GmbH, Hagen, Germany) to achieve a uniformly smooth surface. This embedding and smoothing process was crucial to prevent artefacts such as electron scattering during the subsequent energy-dispersive X-ray spectroscopy (EDX, EDS) analysis.

The embedded samples were cleaned in an ultrasonic bath for five minutes, mounted on SEM sample holders, and sputter-coated with a 5 nm layer of platinum. Elemental composition analysis was carried out using the SEM Zeiss LEO 1525 equipped with an Octane Silicon Drift Detector (SDD) (microanalyses system TEAM, EDAX Inc., New Jersey, USA). For each test, the same settings were applied (e.g., acceleration voltage of 20 kV, same working distance and lens opening). Prior to analysis, the detector was calibrated using copper.
We conducted point analyses (no mapping) on small areas to collect data on various elements present. The detected elements and their proportions included Al (aluminium), C (carbon), Ca (calcium), Cl (chlorine), Cu (copper), Fe (iron), H (hydrogen), K (potassium), Mg (magnesium), N (nitrogen), Na (sodium), O (oxygen), P (phosphorus), Pt (platinum), S (sulphur), Si (silicon), and Zn (zinc). Some elements, such as H, C, N, and O, were not discussed as they constitute the elemental basis of chitin and proteins, while Pt is from the coating and Al and O are from the polishing powder.
For quality control, we performed 10 additional EDX tests on the epoxy to identify any potential contamination arising from mechanical application, embedding, or polishing. No Si (which is present in the sandpaper) or any other elements discussed further as part of the resin's composition were detected. Therefore, their presence was attributed to the teeth.
Due to the overlap between the peaks of phosphorus (P) and platinum (Pt), the software could not reliably distinguish between these two elements. Consequently, the P content was discussed together with Pt (P+Pt). To estimate the proportion of P in the teeth, we measured the Pt content in 20 areas of pure epoxy, yielding a mean value of 0.12 ± 0.02 atomic %. Overall, 416 point measurements of the inner tooth structure were conducted (thereof 140 of natural *D. lacteus*, 136 of *F. affinis*, 140 of the demineralized radulae). After EDX analysis, these samples were used for nanoindentation of the inner tooth structure.

To conduct EDX analyses on the tooth coating towards the oral cavity, we used three radulae of *D. lacteus*, three of *F. affinis*, and two demineralized ones, which were all previously documented by SEM. The same settings and analyses were used as for the inner tooth structure. A total of 798 point measurements (thereof 267 of natural *D. lacteus*, 264 of natural *F. affinis*, 267 of the demineralized radulae) were conducted on the teeth coating towards the oral cavity, distributed across different regions.
To investigate parts located on the underside of the teeth and close to the radular membrane, the radulae were detached from the adhesive carbon tape by 70% EtOH and the Pt coating was removed by an ultrasonic bath in 70% EtOH lasting 30 s. Then, the upper side of the radulae (the tooth cusps and tips) were gently pressed into the adhesive carbon tape on the SEM sample holders. Then, each membrane was grabbed at one side by tweezers and the radula was gently bent. By this, some tooth tips were still attached to the tape, the membrane was bent away and the tooth surface (coating), oriented towards the membrane, was thus visible in the SEM. These tooth surfaces were tested by the EDX. Afterwards, the radulae were detached from the SEM sample holder by 70% EtOH, the Pt coating removed, and the procedure repeated in another area of the radula, to increase the sample size of investigated teeth and to test teeth from different ontogenetic regions. A total of 507 point measurements (thereof 191 of natural *D. lacteus*, 187 of natural *F. affinis*, 129 of the demineralized radulae) were conducted on the coating towards the membrane, distributed across different regions.

Nanoindentation

The mechanical properties of the surfaces (coatings) towards the membrane could not be tested by nanoindentation, because the height of the bent radula hindered the movement of the nanoindenter head across the sample. However, the coating towards the oral cavity and the inner tooth structure, overall 1222 regions, was tested using three radulae of *D. lacteus*, three of *F. affinis*, and two demineralized radulae. These radulae had not previously been used for any other task before (Figure 2). Following the protocol outlined in [118], radulae were carefully ripped into small pieces and attached with their membranes and the teeth handing over the membrane to the nanoindenter sample holder with double sided adhesive tape and air-dried. Important was, that teeth had a large contact area with the tape to avoid movement of the sample during indentation. A nanoindenter SA2 (MTS Nano Instruments, Oak Ridge, Tennessee, USA) equipped with a Berkovich indenter tip and a dynamic contact module (DCM) head was utilized. Hardness (H) and Young's modulus (E) were determined from force-distance curves using the continuous stiffness mode (CSM). All tests were conducted under normal room conditions (relative humidity 28–30%, temperature 22–24 °C), with each indent and corresponding curve manually controlled. The values of E and H were determined at penetration depths ranging from 100 to 300 nm. Approximately 40 values were obtained from the different indentation depths for each site, which were then averaged to calculate one mean H and one mean E value per indent. Overall, the coatings to the oral cavity of 806 localities were tested by nanoindentation (thereof 271 of natural *D. lacteus*, 264 of natural *F. affinis*, 271 of the demineralized radulae).

For the inner tooth structure, the embedded and polished samples were tested. Due to the Pt sputter coating, E and H were determined at penetration depth ranging from 800 to 1000 nm. Overall, 416 localities of the inner structure were tested by nanoindentation (thereof 140 of natural *D. lacteus*, 136 of *F. affinis*, 140 of the demineralized *D. lacteus* radulae).

Statistical analyses

All statistical analyses were conducted using JMP Pro, Version 14 (SAS Institute Inc., Cary, NC, 1989–2007). Mean values and standard deviations were calculated, and the Shapiro-Wilk test was employed to assess normality. Since the data was found to be non-normally distributed, a Kruskal-Wallis test was performed. Subsequently, pairwise comparisons were conducted using the Wilcoxon method. Correlation coefficients and relationships between parameters were calculated with JMP as well.

Supporting Information

File (Supplementary Material, PDF file format) with correlation coefficients, results from nanoindentation and elemental analysis.

Declarations

Ethics approval and consent to participate. Not applicable.

Consent for publication. Not applicable

Data Availability Statement. The data on mechanical properties and elemental analysis can be found in the Supplementary Material.

Competing interests. The authors declare that they have no competing interests

Funding. This research was financed by the Deutsche Forschungsgemeinschaft (DFG) grant 470833544 to WK.

Authors' contributions. WK, SG, and HW initiated the study. WK performed nanoindentation, WK and CN performed SEM and EDX analyses. WK wrote the first draft of the manuscript. All authors contributed to and approved the final version of the manuscript for publication.

Acknowledgements. We would like to thank Elke Woelken from the Institute of Cell and Systems Biology of Animals, Universität Hamburg, for her support on the SEM and Alexander Koehnsen, Christian-Albrechts-University zu Kiel, for the modelling of the radular teeth. We are highly grateful for the helpful comments of the anonymous reviewers.

References

1. Wägele, H.; Klussmann-Kolb, A. *Front. Zool.* **2005**, *2* (1), 3.
2. Aboul-Ela, I. A. *Biol. Bull.* **1959**, *117*, 439–442.
3. McBeth, J. *Veliger* **1971**, *14*, 158–161.
4. McDonald, G. R.; Nybakken, J. W. *Veliger* **1978**, *21*, 110–119.
5. Cattaneo-Vietti, R.; Balduzzi, A. *Malacologia* **1991**, *32*, 211–217.
6. Johnson, S. *Hawaiian Shell News* **1992**, *40* (2), 3–6.
7. Valdés, Á. *Biol. J. Linn. Soc.* **2004**, *83*, 551–559.
8. Göbbeler, K.; Klussmann-Kolb, A. *Thalassas* **2011**, *27*, 121–154.
9. Nakano, R.; Hirose, E. *Veliger* **2011**, *51*, 66.
10. Goodheart, J. A.; Bazinet, A. L.; Valdés, Á.; Collins, A. G.; Cummings, M. P. *BMC Evol. Biol.* **2017**, *17*, 221.
11. Hertzer, C.; Kehraus, S.; Böhringer, N.; Kaligis, F.; Bara, R.; Erpenbeck, D.; Wörheide, G.; Schäberle, T. F.; Wägele, H.; König, G. M. *Beilstein J. Org. Chem.* **2020**, *16*, 1596–1605.
12. Mikhlina, A.; Ekimova, I.; Vortsepneva, E. *Zoology* **2020**, *143*, 125850.
13. Solem, A. *Veliger* **1972**, 14, 327–336.
14. Solem, A. *The shell makers: Introducing mollusks*; Jon Wiley & Sons: New York, U.S.A., 1974.
15. Steneck, R. S.; Watling, L. *Mar. Biol.* **1982**, *68*, 299–319.
16. Hawkins, S. J.; Watson, D. C.; Hill, A. S.; Harding, S. P.; Kyriakides, M. A.; Hutchinson, S.; Norton, T. A. *J. Molluscan Stud.* **1989**, *55* (2), 151–165.
17. Padilla, D. K. *Am. Malacol. Bull.* **2003**, *18* (1–2), 163–168.
18. Ukmar-Godec, T.; Kapun, G.; Zaslansky, P.; Faivre, D. *J. Struct. Biol.* **2015**, *192*, 392–402.
19. Krings, W.; Marcé-Nogué, J.; Karabacak, H.; Glaubrecht, M.; Gorb, S. N. *Acta Biomater.* **2020a**, *115*, 317–332.
20. Krings, W.; Kovalev, A.; Gorb, S. N. *Proc. R. Soc. B* **2021a**, *288*, 20203173.
21. Krings, W.; Marcé-Nogué, J.; Gorb, S. N. *Sci. Rep.* **2021b**, *11*, 22775.
22. Krings, W.; Karabacak, H.; Gorb, S. N. *J. R. Soc. Interface* **2021c**, *18* (182), 20210377.
23. Krings, W.; Gorb, S. N. *J. Molluscan Stud.* **2021a**, *87*, eyab007.
24. Filippov, A. E.; Gorb, S. N.; Kovalev, A. E.; Krings, W. *Adv. Theory Simul.* **2023**, *6*, 2300055.
25. Krings, W.; Brütt, J.-O.; Gorb, S. N.; Glaubrecht, M. *Malacologia* **2020b**, *63* (1), 77–94.
26. Krings, W.; Brütt, J.-O.; Gorb, S. N. *Philos. Trans. R. Soc. A* **2022a**, *380*, 20210335.
27. Krings, W.; Gorb, S. N. *J. Chem. Phys.* **2023a**, *159* (18), 185101.
28. Padilla, D. K. *Mar. Biol.* **1985**, *90*, 103–109.
29. Padilla, D. K. *Ecology* **1989**, *70*, 835–842.
30. Weaver, J. C.; Wang, Q.; Miserez, A.; Tantuccio, A.; Stromberg, R.; Bozhilov, K. N.; Maxwell, P.; Nay, R.; Heier, S. T.; DiMasi, E. *Mater. Today* **2010**, *13* (1–2), 42–52.
31. Lu, D.; Barber, A. H. *J. Royal. Soc. Interface* **2012**, *9* (71), 1318–1324.
32. Barber, A. H.; Lu, D.; Pugno, N. M. *J. Royal. Soc. Interface* **2015**, *12* (105), 20141326.
33. Herrera, S. A.; Grunenfelder, L.; Escobar, E.; Wang, Q.; Salinas, C.; Yaraghi, N.; Geiger, J.; Wuhrer, R.; Zavattieri, P.; Kisailus, D. Stylus support structure and function of radular teeth in *Cryptochiton stelleri*. *20th International Conference on Composite Materials*, Copenhagen, D.K., July 19–24th, 2015.
34. Ukmar-Godec, T.; Bertinetti, L.; Dunlop, J. W. C.; Godec, A.; Grabiger, M. A.; Masic, A.; Nguyen, H.; Zlotnikov, I.; Zaslansky, P.; Faivre, D. *Adv. Mater.* **2017**, *29* (27), 1701171.
35. Krings, W.; Kovalev, A.; Glaubrecht, M.; Gorb, S. N. *Zoology* **2019a**, *137*, 125713.
36. Krings, W.; Neiber, M. T.; Kovalev, A.; Gorb, S. N.; Glaubrecht, M. *BMC Ecol. Evol.* **2021d**, *21*, 35.
37. Krings, W.; Brütt, J.-O.; Gorb, S. N. *Front. Zool.* **2022b**, *19*, 19.

38. Krings, W.; Matsumura, Y.; Brütt, J.-O.; Gorb, S. N. *Sci. Nat.* **2022c**, *109*, 52.
39. Krings, W.; Neumann, C.; Gorb, S. N.; Koehnsen, A.; Wägele, H. *Ecol. Evol.* **2023a**, *13*, e10332.
40. Krings, W.; Wägele, H.; Neumann, C.; Gorb, S. N. *J. R. Soc. Interface* **2023b**, *20*, 20220927.
41. Pohl, A.; Herrera, S. A.; Restrepo, D.; Negishi, R.; Jung, J.-Y.; Salinas, C.; Wuhrer, R.; Yoshino, T.; McKittrick, J.; Arakaki, A.; Nemoto, M.; Zavattieri, P.; Kisailus, D. *J. Mech. Behav. Biomed. Mater.* **2020**, *111*, 103991.
42. Krings, W. Trophic specialization of paludomid gastropods from 'ancient' Lake Tanganyika reflected by radular tooth morphologies and material properties. Ph. D. Thesis, University of Hamburg, Germany, 2020.
43. Gorb, S. N.; Krings, W. *Acta Biomater.* **2021**, *134* (15), 513–530.
44. Hackethal, S.; Schulz-Kornas, E.; Gorb, S. N.; Krings, W. Interface Focus **2024**, *14*, 20230082.
45. Hickman, C. S. *Paleobiology* **1980**, *6* (3), 276–294.
46. Hickman, C. S. *Malacologia* **1984**, *25* (1), 143–160.
47. Krings, W.; Kovalev, A.; Gorb, S. N. *Acta Biomater.* **2021e**, *135*, 458–472.
48. van der Wal, P.; Giesen, H. J.; Videler, J. J. *Mater. Sci. Eng. C* **1999**, *7* (2), 129–142.
49. Wealthall, R. J.; Brooker, L. R.; Macey, D. J.; Griffin, B. J. *J. Morphol.* **2005**, *265*, 165–175.
50. Shaw, J. A.; Macey, D. J.; Brooker, L. R.; Stockdale, E. J.; Saunders, M.; Clode, P. L. *J. Morphol.* **2009a**, *270*, 588–600.
51. Shaw, J. A.; Macey, D. J.; Brooker, L. R.; Stockdale, E. J.; Saunders, M.; Clode, P. L. *Microsc. Microanalysis* **2009b**, *15* (2), 154–165.
52. Shaw, J. A.; Macey, D. J.; Brooker, L. R.; Clode, P. L. *Biol. Bull.* **2010**, *218* (2), 132–144.
53. Saunders, M.; Kong, C.; Shaw, J. A.; Clode, P. L. *Microsc. Microanal.* **2011**, *17*, 220–225.
54. Han, Y.; Liu, C.; Zhou, D.; Li, F.; Wang, Y.; Han, X. *Bioelectromagnetics* **2011**, *32*, 226–233.
55. Wang, C.; Li, Q. Y.; Wang, S. N.; Qu, S. X.; Wang, X. X. *Mater. Sci. Eng. C* **2014**, *37*, 1–8.
56. Runham, N. W. *Q. J. Microsc. Sci.* **1961**, *102*, 371–380.
57. Evans, L. A.; Macey, D. J.; Webb, J. *Mar. Biol.* **1991**, *109*, 281–286.
58. Guralnick, R.; Smith, K. *J. Morphol.* **1999**, *241*, 175–195.
59. Mackenstedt, U.; Märkel, K. Radular structure and function. In *The Biology of Terrestrial Molluscs*; Barker, G. M., Ed.; CABI Publishing, Oxon, U.K., 2001; pp. 213–236.
60. Katsuno, S.; Sasaki, T. *Malacologia* **2008**, *50* (1–2), 13–56.
61. Golding, R. E.; Ponder, W. F.; Byrne, M. *J. Morphol.* **2009**, *270*, 558–587.
62. Neustadter, D. M.; Drushel, R. F.; Crago, P. E.; Adams, B. W.; Chiel, H. J. *J. Exp. Biol.* **2002**, *205*, 3177–3206.
63. Kehl, C. E.; Wu, J.; Lu, S.; Neustadter, D. M.; Drushel, R. F.; Smoldt, R. K.; Chiel, H. J. *J. Exp. Biol.* **2019**, *222*, jeb191254.
64. Montroni, D.; Zhang, X.; Leonard, J.; Kaya, M.; Amemiya, C.; Falini, G.; Rolandi, M. *PLoS One* **2019**, *14* (8), e0212249.
65. Krings, W.; Gorb, S. N. *Biotribology* **2021b**, *26*, 100164.
66. Krings, W.; Hempel, C.; Siemers, L.; Neiber, M. T.; Gorb, S. N. *Sci. Rep.* **2021f**, *11*, 9556.
67. Mikhlina, A.; Tzetlin, A.; Vortsepneva, E. *Zoomorphology* **2018**, *137*, 31–50.
68. Vortsepneva, E.; Mikhlina, A., Kantor, Y. *J. Morphol.* **2022**, *284*, e21538
69. Mikhlina, A.; Vortsepneva, E. *J. Morphol.* **2023**, *284*, e21593.
70. Krings, W.; Gorb, S. N. *Invertebr. Biol.* **2023b**, *142* (3), e12410.
71. Schmekel, L.; Portmann, A. *Opisthobranchia des Mittelmeeres*; Springer Verlag: Berlin Heidelberg New York, 1982.
72. Ekimova, I.; Korshunova, T.; Schepetov, D.; Neretina, T.; Sanamyan, N.; Martynov, A. *Zool. J. Linn. Soc.* **2015**, *173*, 841–886.
73. Mikhlina, A. L.; Vortsepneva, E. V.; Tzetlin, A. B. *Invertebrate Zoology* **2015**, *12* (2), 175–196.
74. Ekimova, I.; Valdés, Á.; Chichvarkhin, A.; Antokhina, T.; Lindsay, T.; Schepetov, D. *Mol. Phylogenetics Evol.* **2019**, *141*, 106609.
75. Bendsøe, M. P.; Kikuchi, N. *Comput. Methods Appl. Mech. Eng.* **1988**, *71*, 197–224.

76. Bendsøe, M. P. *Struct Optim* **1989**, *1*, 193–202.
77. Bendsøe, M. P. *Optimization of structural topology. Shape and material*; Springer: Berlin, Germany, 1995.
78. Dumont, E. R.; Grosse, I. R.; Slater, G. J. *J. Theor. Biol.* **2009**, *256*, 96–103.
79. Freeman, P. W.; Lemen, C. A. *J. Zool.* **2007**, *273*, 273–280.
80. Anderson, P. S. L. *J. Exp. Biol.* **2018**, *221* (22), jeb187294.
81. Scheel, C.; Gorb, S. N.; Glaubrecht, M.; Krings, W. *Biol. Open* **2020**, *9*, bio055699.
82. Krings, W.; Faust, T.; Kovalev, A.; Neiber, M. T.; Glaubrecht, M.; Gorb, S. N. *R. Soc. Open Sci.* **2019b**, *6* (7), 2054–5703.
83. Krings, W.; Neumann, C.; Neiber, M. T.; Kovalev, A.; Gorb, S. N. *Sci. Rep.* **2021g**, *11*, 10560.
84. Liu, Z.; Meyers, M. A.; Zhang, Z.; Ritchie, R. O. *Progr. Mater. Sci.* **2017**, *88*, 467–98.
85. Brooker, L. R.; Shaw, J. A. The chiton radula: A unique model for biomineralization studies. In *Advanced topics in biomineralization*; Seto, J., Ed.; Intech Open: Rijeka, Croatia, 2012: pp 65–84.
86. Faivre, D.; Ukmar-Godec, T. *Angew. Chem. Int. Ed. Engl.* **2015**, *54*, 4728–4747.
87. Joester, D.; Brooker, L. R. The chiton radula: A model system for versatile use of iron oxides. In *Iron oxides: From nature to applications*; Faivre, D., Ed.; Wiley-VCH: Weinheim, Germany, 2016; pp 177–205.
88. Grunenfelder, L. K.; de Obaldia, E. E.; Wang, Q.; Li, D.; Weden, B.; Salinas, C.; Wuhrer, R.; Zavattieri, P.; Kisailus, D. *Adv. Funct. Mater.* **2014**, *24* (39), 6093–6104.
89. Kirschvink, J. L.; Lowenstam, H. A., *EPSL* **1979**, *44*, 193–204.
90. Michels, J.; Gorb, S. N. *J. Microsc.* **2012**, *245*, 1–16.
91. Michels, J.; Appel, E.; Gorb, S. N. *Beilstein J. Nanotechnol.* **2016**, *7*, 1241–1259.
92. Michels, J.; Vogt, J.; Gorb, S. N. *Sci. Rep.* **2012**, *2*, 465.
93. Michels, J.; Gorb, S. N. Mandibular gnathobases of marine planktonic copepods — Structural and mechanical challenges for diatom frustules in evolution of lightweight structures. In *Evolution of lightweight structures*; Hamm, C., Ed.; Springer: Dordrecht, Netherlands, 2015; pp 59–73.
94. Krings, W.; Brütt, J.-O.; Gorb, S. N. *Sci. Rep.* **2022e**, *12*, 17799.
95. Lowenstam, H. A. *Science* **1967**, *56*, 1373–1375.
96. Lowenstam, H. A.; Weiner, S. *Science* **1985**, *227*, 51–52.
97. Brooker, L. R.; Macey, D. J. *Am. Malacol. Bull.* **2011**, *16*, 203–215.
98. Brooker, L. R.; Lee, A. P.; Macey, D. J.; van Bronswijk, W.; Webb, J. *Mar. Biol.* **2003**, *142*, 447–454.
99. Shaw, J. A.; Macey, D. J.; Brooker, L. R. *J. Mar. Biolog. Assoc. U.K.* **2008**, *88*, 597–601.
100. Krings, W.; Brütt, J.-O.; Gorb, S. N. *Sci. Rep.* **2022d**, *12*, 7499.
101. Creighton, T. E. *Biol. Chem.* **1997**, *378*, 731–744.
102. Harding, M. M. *Acta Cryst. D* **2002**, 58, 872–874.
103. Lowenstam, H. A. *Geol. Soc. Am. Bull.* **1962**, *73*, 435–438.
104. Lowenstam, H. A.; Weiner, S. Mollusca. In *On biomineralization*; Lowenstam, H.A.; Weiner, S., Eds.; Oxford University Press: Oxford, U.K., 1989; pp 88–305.
105. Huang, C.; Li, C.-W.; Deng, M.; Chin, T. *IEEE Trans. Magn.* **1992**, *28*, 2409–2411.
106. Wang, Q.; Nemoto, M.; Li, D.; Weaver, J. C.; Weden, B.; Stegemeier, J.; Bozhilov, K. N.; Wood, L. R.; Milliron, G. W.; Kim, C. S.; DiMasi, E.; Kisailus, D. *Adv. Funct. Mater.* **2013**, *23*, 2908–2917.
107. Ukmar-Godec, T. Mineralization of goethite in limpet radular teeth. In *Iron oxides: from nature to applications*; Faivre, D., Ed.; Wiley-VCH: Weinheim, Germany, 2016; pp 207–224.
108. McCoey, J. M.; Matsuoka, M.; Gille, R. W. de; Hall, L. T.; Shaw, J. A.; Tetienne, J.-P.; Kisailus, D.; Hollenberg, L. C. L.; Simpson, D. A. *Small Methods* **2020**, *4*, 1900754.
109. Macey, D. J.; Brooker, L. R. *J. Morphol.* **1996**, *230*, 33–42.

110. Hua, T.-E.; Li, C.-W. *Zool. Stud.* **2007**, *46*, 379–388.
111. Houbrick, J. R.; Fretter, V. *J. Molluscan Stud.* **1969**, *38* (5), 415–429.
112. Fänge, R.; Lidman, U. *Comp. Biochem. Physiol.* **1976**, *53* (1), 101–103.
113. Morton, B. *J. Molluscan Stud.* **1990**, *56* (4), 477–486.
114. Morton, B. *J. Nat. Hist.* **2015**, *49* (9–10), 483–507.
115. Moura, K. R. S.; Terra, W. R.; Ribeiro, A. F. *J. Molluscan Stud.* **2004**, *70* (1), 21–29.
116. Brütt, J.-O.; Gorb, S. N.; Krings, W. *Sci. Nat.* **2022**, *109*, 58.
117. Krings, W.; Below, P.; Gorb, S. N. *Sci. Rep.* **2024**, *14*, 4695.
118. Krings, W.; Gorb, S. N. *Zoomorphology* **2023c**, *142*, 423–438.

Figures and legends

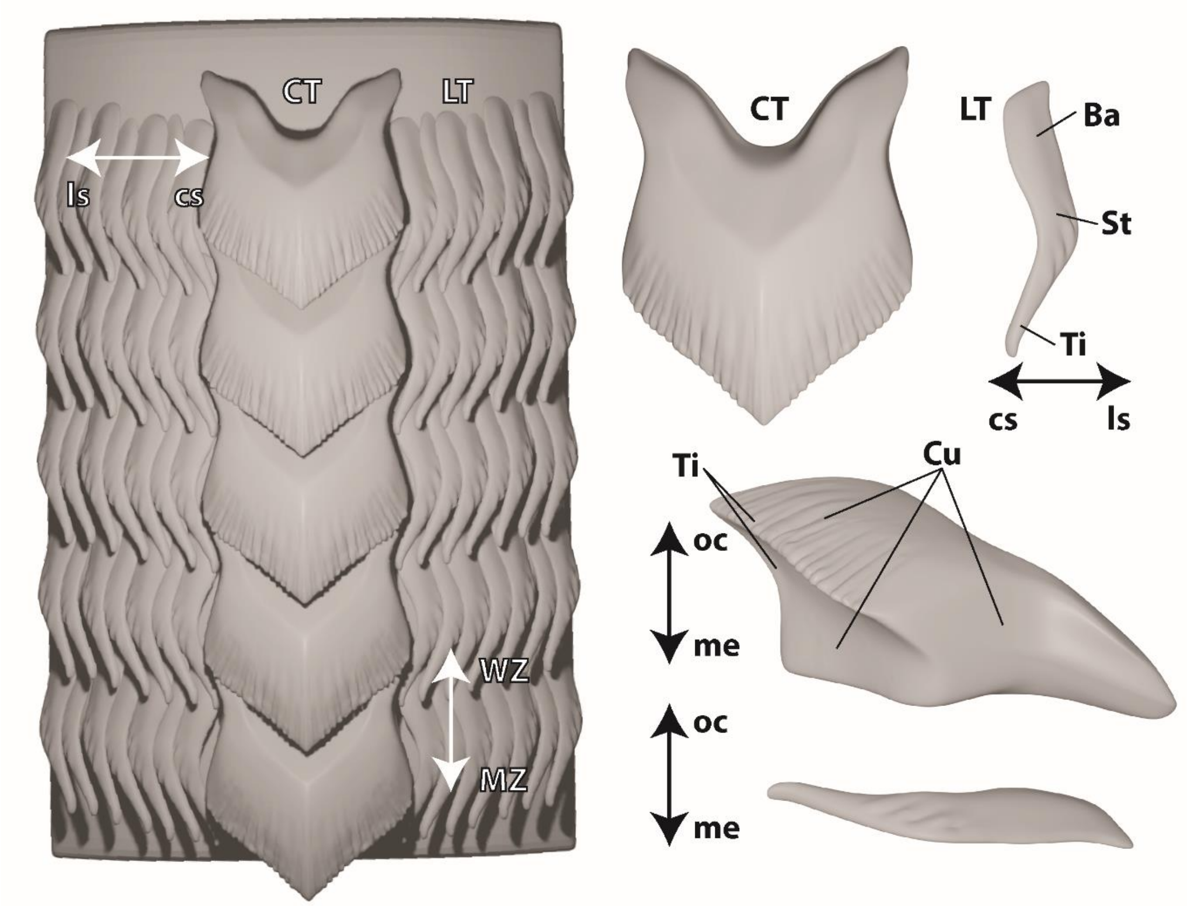

Figure 1. 3-dimensional model of the *Dendronotus lacteus* radula in frontal and lateral views, displaying the regions of interest. Abbreviations: Ba, tooth basis; cs, side of the lateral teeth facing the central (rhachidian) tooth; CT, central tooth (rhachidian); ls, outer/lateral side of the lateral teeth; LT, lateral tooth; me, tooth coating towards the radular membrane; oc, tooth coating towards the oral cavity; St, tooth stylus; Ti, tooth tip; WZ, working zone.

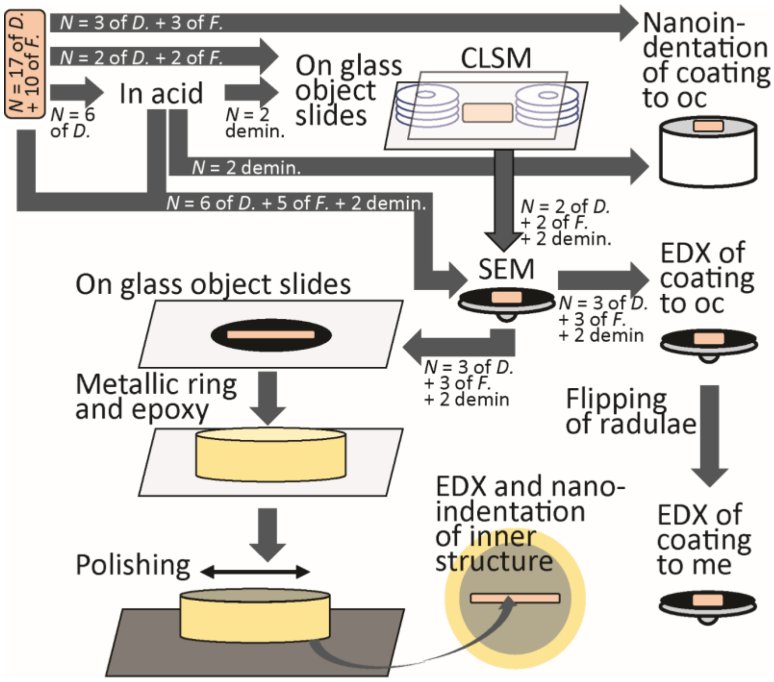

Figure 2. Workflows used in the study. Overall, 17 radulae of *Dendronotus lacteus* and 10 of *Flabellina affinis* were mechanically extracted and subsequently treated differently to perform CLSM, SEM, EDX, and nanoindentation analyses. Different experimental pathways were necessary, to not allow to use the same radula for another analysis (e.g., the sputter coating from SEM hinders CLSM analysis or the nanoindentation of the coating towards the oral cavity). Abbreviations: CLSM, confocal laser scanning microscopy; *D.*, *D. lacteus*; Demin., demineralized; EDX, energy-dispersive X-ray spectroscopy; *F.*, *F. affinis*; me, membrane; *N*, number of radulae used; oc, oral cavity; SEM, scanning electron microscopy.

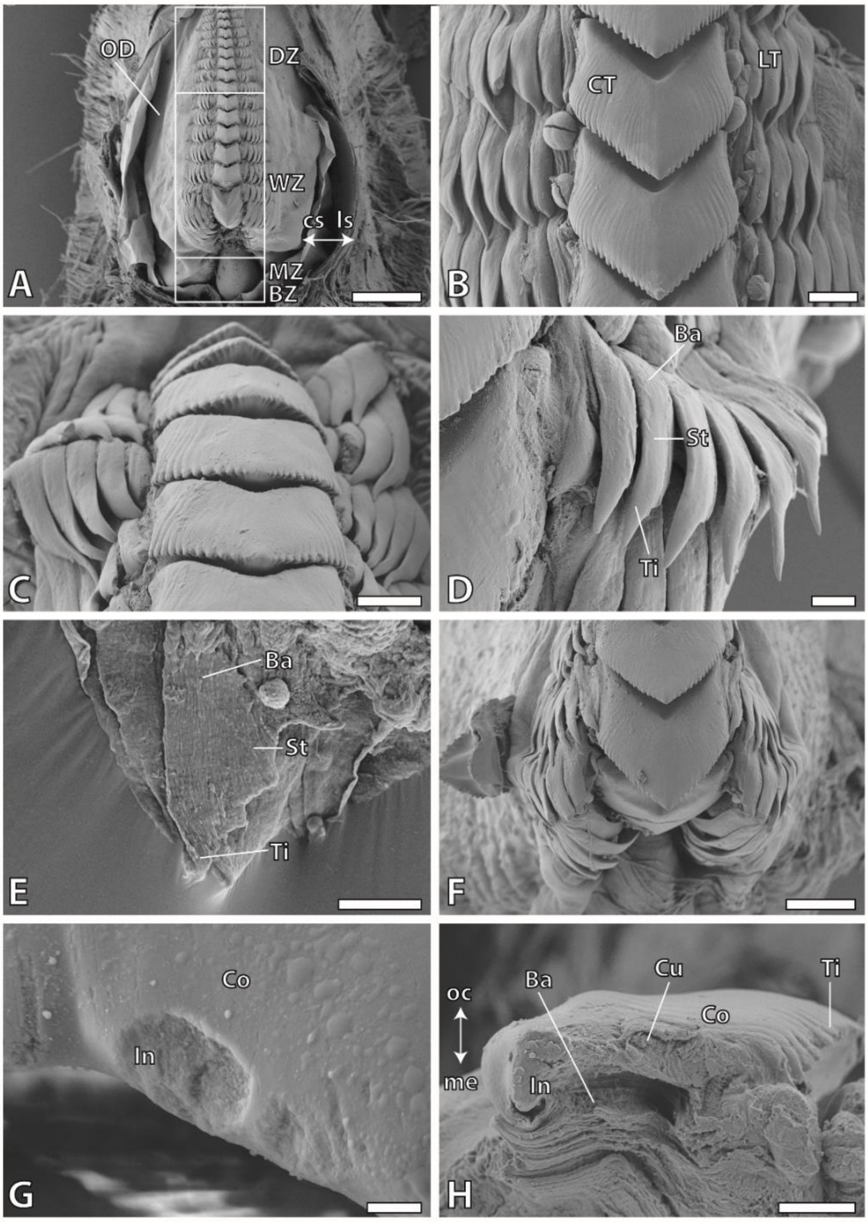

Figure 3. SEM images of natural radulae (not demineralized) of *Dendronotus lacteus*. A. Overview of one critically-point dried radula showing the working zone and degeneration zone with attached odontophoral cartilage. The maturation zone and building zone are located underneath the working zone. B–D. Magnifications of the central and lateral teeth. E. Surface of the lateral teeth towards the membrane. These surfaces are less smooth and more fibrous than the surfaces towards the oral cavity. F. Magnification of the radular working zone of one critically-point dried radula. G. Surface (coating) of one central tooth. H. Central tooth, broken with tweezers, to show the fibrous inner tooth structure, the tooth's anchorage in the membrane, and the smooth coating. Abbreviations: Ba, tooth basis; Co, tooth coating; cs, side of the lateral teeth facing the central (rhachidian) tooth; CT, central tooth; Cu, tooth cusp; DZ, degenerative zone; In, inner structure of tooth; ls, outer/lateral side of the lateral teeth; LT, lateral tooth; me, tooth coating towards the radular membrane; MZ, maturation zone; oc, tooth coating towards the oral cavity; St, tooth stylus; Ti, tooth tip; OD, odontophoral cartilage; WZ, working zone. Scale bars: A, 200 µm; B, C, 40 µm; D, E, H, 20 µm; F, 80 µm; G, 2 µm.

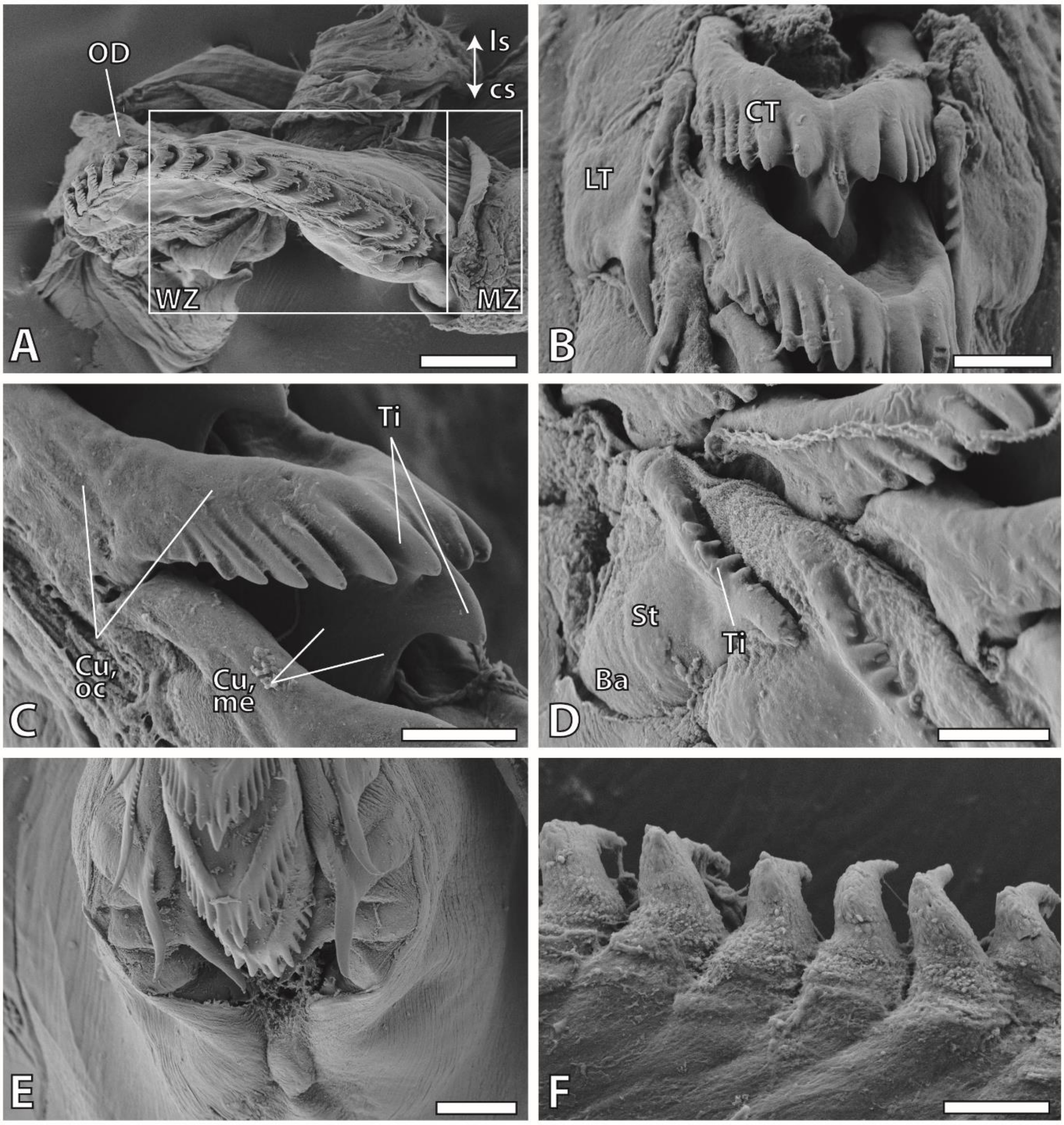

Figure 4. SEM images of radulae of *Flabellina affinis*. A. Overview of one radula with attached odontophoral cartilage. The maturation and building zone is still covered by the epithelium that forms the teeth. B–D. Magnifications of the central and lateral teeth. E. Magnification of the radular working zone of one critically-point dried radula. F. Denticles of the masticatory processus of the jaw. Abbreviations: Ba, tooth basis; cs, side of the lateral teeth facing the central (rhachidian) tooth; CT, central tooth; Cu, tooth cusp; ls, outer/lateral side of the lateral teeth; LT, lateral tooth; me, tooth coating towards the radular membrane; MZ, maturation zone; oc, tooth coating towards the oral cavity; OD, odontophoral cartilage; St, tooth stylus; Ti, tooth tip; WZ, working zone. Scale bars: A, 100 µm; B, C, D, 10 µm; E, 20 µm.

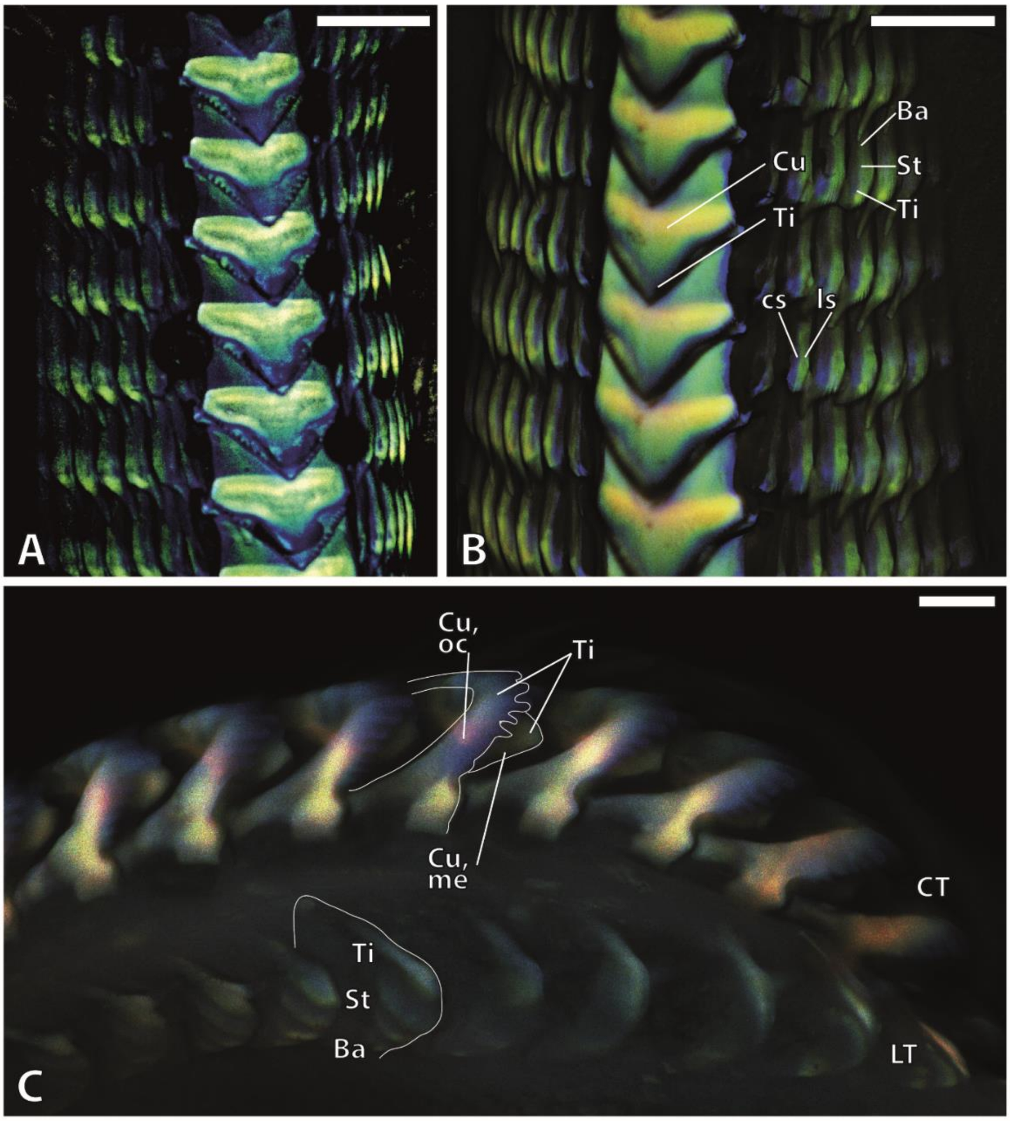

Figure 5. CLSM images of one natural *Dendronotus lacteus* radula (A), one demineralized *D. lacteus* radula (B) and one natural *Flabellina affinis* radula (C). Abbreviations: Ba, tooth basis; Cu, tooth cusp; cs, side of the lateral teeth facing the central (rhachidian) tooth; CT, central tooth; ls, outer/lateral side of the lateral teeth; LT, lateral tooth; me, tooth coating towards the radular membrane; St, tooth stylus; Ti, tooth tip; oc, tooth coating towards the oral cavity. Scale bars: A, B, 120 µm; C, 30 µm.

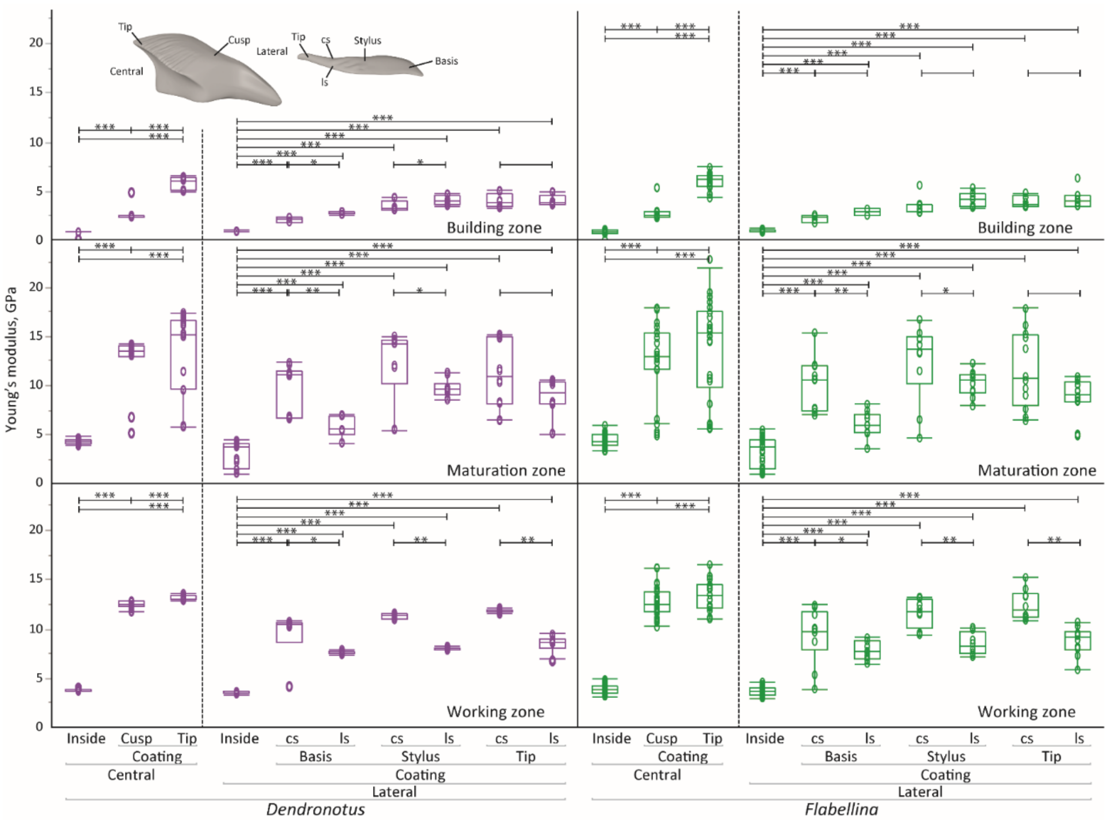

Figure 6. The results from nanoindentation experiments. The Young's modulus *E* (in GPa) for the natural radulae of *Dendronotus lacteus* and *Flabellina affinis*. The statistical results are from pairwise comparison. Abbreviations: cs, side of the lateral teeth facing the central (rhachidian) tooth; ls, outer/lateral side of the lateral teeth.

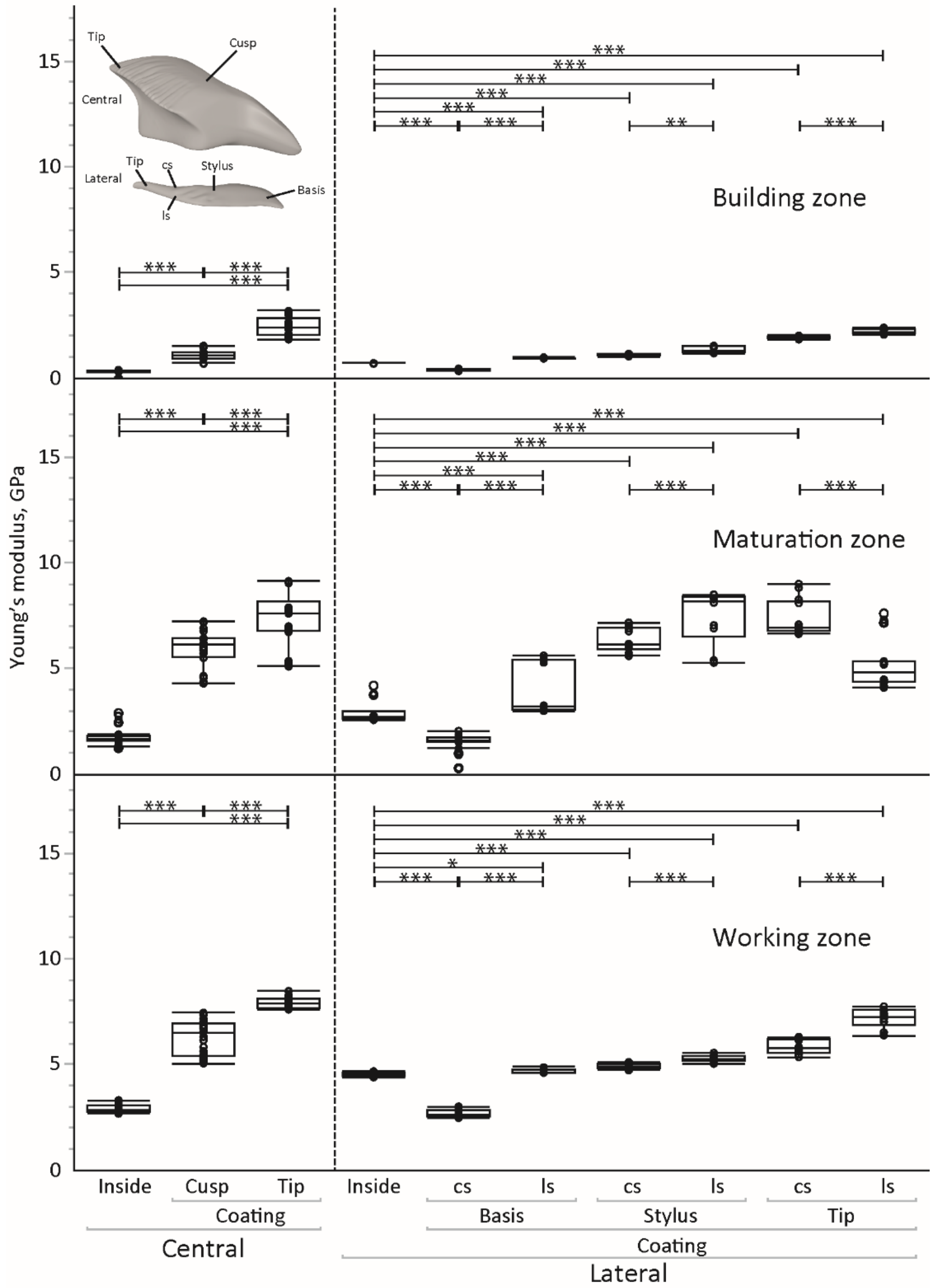

Figure 7. The results from nanoindentation experiments. The Young's modulus *E* (in GPa) for demineralized radulae of *Dendronotus lacteus*. The statistical results are from pairwise comparison. Abbreviations: cs, side of the lateral teeth facing the central (rhachidian) tooth; ls, outer/lateral side of the lateral teeth.

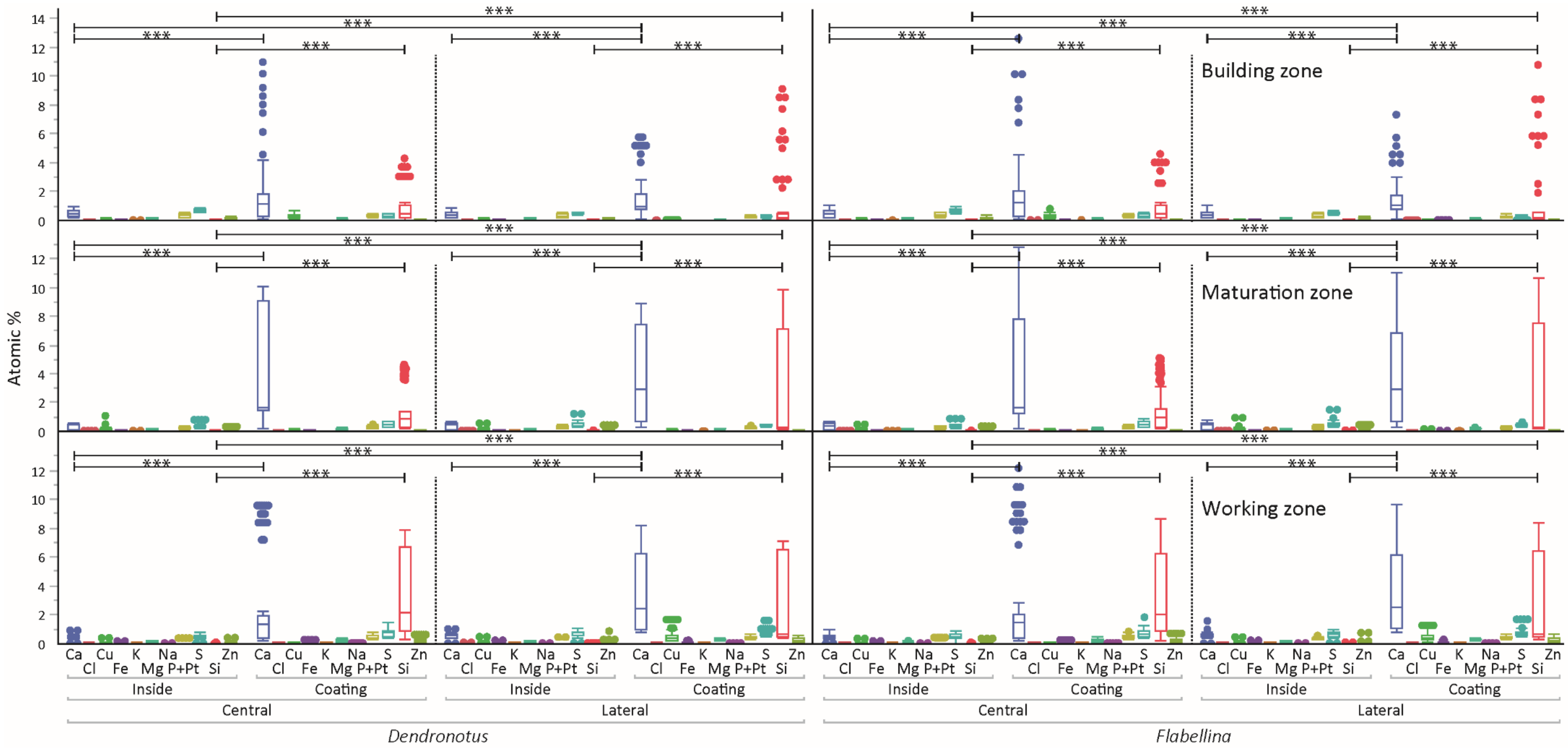

Figure 8. The results from the EDX analysis of natural radulae *of Dendronotus lacteus* and *Flabellina affinis*. For each of the discussed elements, the results are given in atomic %. The statistical results are from pairwise comparison.

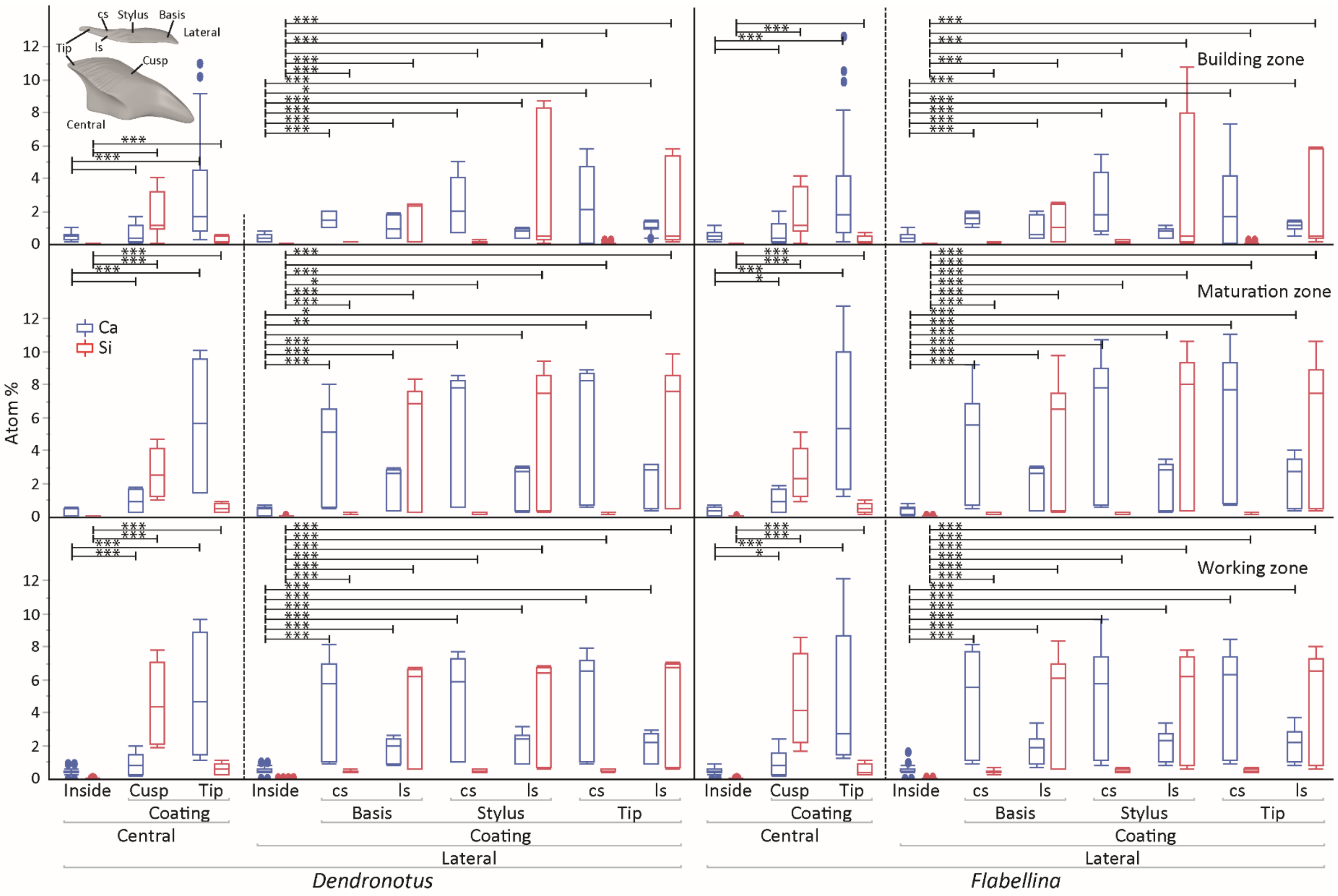

Figure 9. The results from the EDX analysis for Ca and Si in natural radulae of *Dendronotus lacteus* and *Flabellina affinis*. The results are given in atomic %. The results of the coating towards the oral cavity and towards the membrane are pooled together. The statistical results are from pairwise comparison. Abbreviations: cs, side of the lateral teeth facing the central (rhachidian) tooth; ls, outer/lateral side of the lateral teeth.

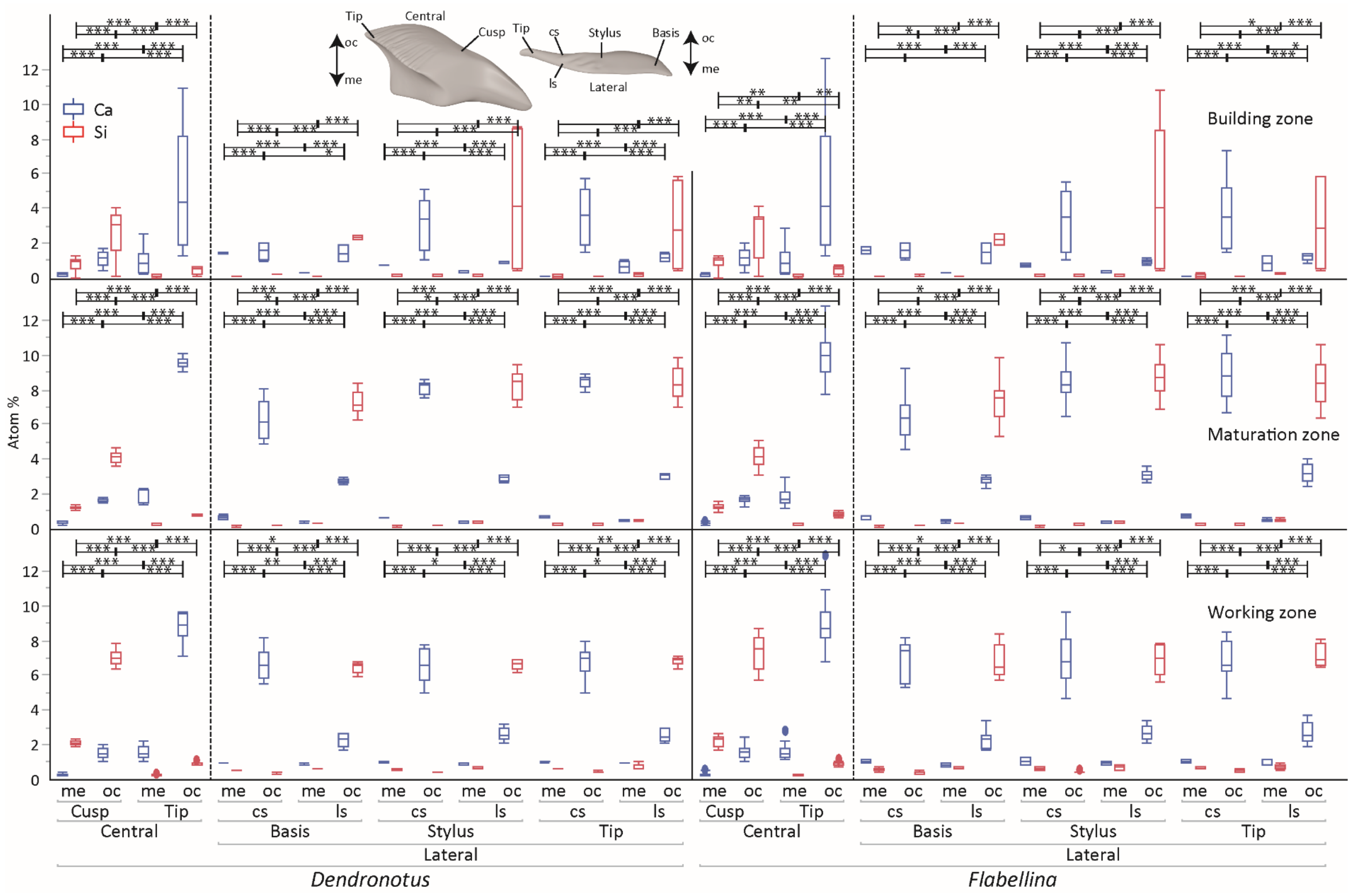

Figure 10. The results from the EDX analysis for Ca and Si of coatings of the natural radulae in *Dendronotus lacteus* and *Flabellina affinis.* The results are given in atomic %. The results of the coating towards the oral cavity and towards the membrane are not pooled together. The statistical results are from pairwise comparison. Abbreviations: cs, side of the lateral teeth facing the central (rhachidian) tooth; ls, outer/lateral side of the lateral teeth; me, tooth coating towards the membrane; oc, tooth coating towards the oral cavity.

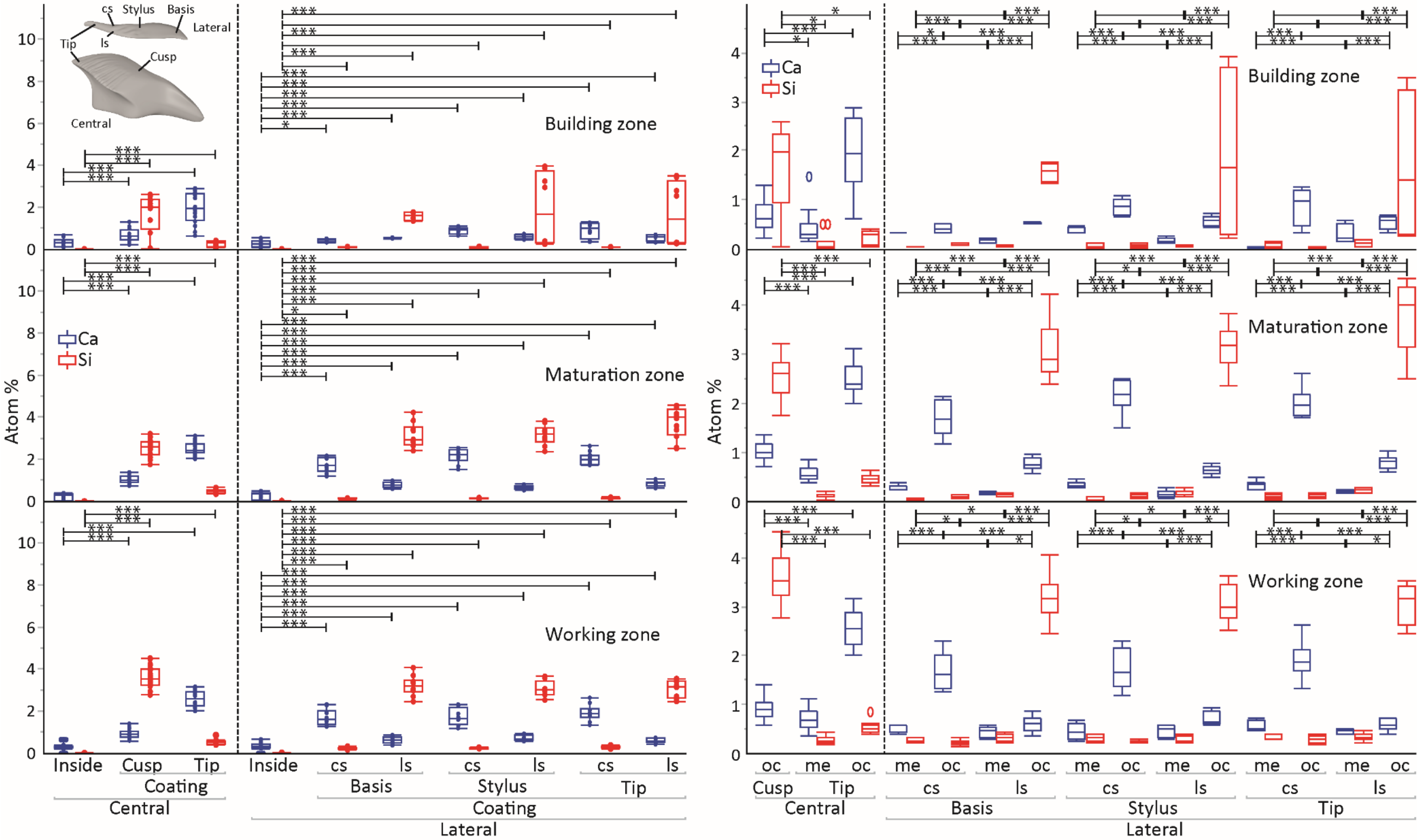

Figure 11. The results from the EDX analysis in demineralized radulae of *Dendronotus lacteus.* The results for Ca and Si are given in atomic %. Left side: The results of the coating towards the oral cavity and towards the membrane are pooled together. Right side: Only the coating is plotted. The EDX results on the coating towards the oral cavity and towards the membrane are not pooled together. The statistical results are from pairwise comparison. Abbreviations: cs, side of the lateral teeth facing the central (rhachidian) tooth; ls, outer/lateral side of the lateral teeth; me, tooth coating towards the membrane; oc, tooth coating towards the oral cavity.

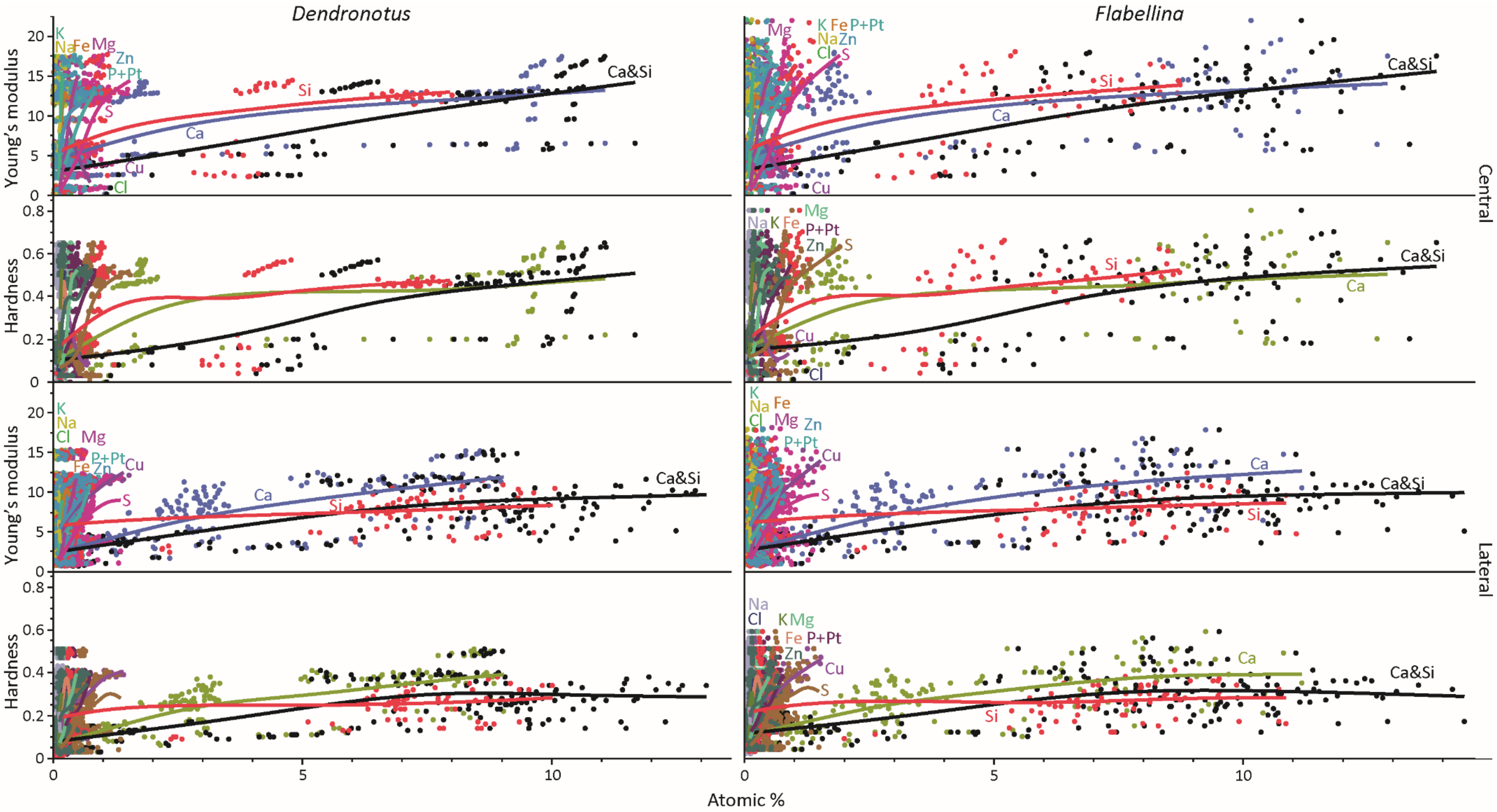

Figure 12. *Dendronotus lacteus* and *Flabellina affinis*, natural radulae. Relationship between the hardness (*H*) and Young's modulus (*E*), both given in GPa. The EDX results on discussed elements are given in atomic %. The amount of Ca and Si show a clear positive relationship with the mechanical properties.